THE UNIVERSITY OF WARWICK

Permanent WRAP url:
http://wrap.warwick.ac.uk/74794

A note on versions:
The version presented in WRAP is the published version, or, version of record, and may be cited as it appears here.

For more information, please contact the WRAP Team at: publications@warwick.ac.uk

warwickpublicationswrap

highlight your research

http://wrap.warwick.ac.uk/

The effect of oxide precipitates on minority carrier lifetime in *n*-type silicon

J. D. Murphy,[1,a)] M. Al-Amin,[1] K. Bothe,[2] M. Olmo,[3] V. V. Voronkov,[4] and R. J. Falster[3]

[1]*School of Engineering, University of Warwick, Coventry CV4 7AL, United Kingdom*
[2]*Institut für Solarenergieforschung Hameln/Emmerthal, Am Ohrberg 1, 31860 Emmerthal, Germany*
[3]*SunEdison Semiconductor, Viale Gherzi 31, 28100 Novara, Italy*
[4]*SunEdison Semiconductor, Via Nazionale 59, 39012 Merano, Italy*

Supersaturated levels of interstitial oxygen in Czochralski silicon can lead to the formation of oxide precipitates. Although beneficial from an internal gettering perspective, oxygen-related extended defects give rise to recombination which reduces minority carrier lifetime. The highest efficiency silicon solar cells are made from *n*-type substrates in which oxide precipitates can have a detrimental impact on cell efficiency. In order to quantify and to understand the mechanism of recombination in such materials, we correlate injection level-dependent minority carrier lifetime data measured with silicon nitride surface passivation with interstitial oxygen loss and precipitate concentration measurements in samples processed under substantially different conditions. We account for surface recombination, doping level, and precipitate morphology to present a generalised parameterisation of lifetime. The lifetime data are analysed in terms of recombination activity which is dependent on precipitate density or on the surface area of different morphologies of precipitates. Correlation of the lifetime data with interstitial oxygen loss data shows that the recombination activity is likely to be dependent on the precipitate surface area. We generalise our findings to estimate the impact of oxide precipitates with a given surface area on lifetime in both *n*-type and *p*-type silicon. © *2015 Author(s). All article content, except where otherwise noted, is licensed under a Creative Commons Attribution 3.0 Unported License.*
[http://dx.doi.org/10.1063/1.4936852]

I. INTRODUCTION

Czochralski silicon (Cz-Si) usually contains 10^{17}–10^{18} cm^{-3} of interstitial oxygen, which is incorporated from the walls of the silica crucible which contains the melt. At typical processing temperatures, the oxygen is supersaturated and this provides a driving force for precipitation. Precipitate nuclei can be formed intentionally by careful thermal processing, and in silicon for integrated circuits, oxide precipitates are deliberately formed away from the active region of a device to provide *internal gettering* centres for harmful metallic impurities.[1,2] Oxide precipitates initially form as unstrained particles and, as they grow, they undergo a morphological transformation into strained ones.[3,4] As precipitates grow with further processing, dislocations and/or stacking faults can form around the oxide precipitates. The precipitates must be strained in order for them to getter impurities.[4]

The relatively fast crystal pulling rates often used in silicon for photovoltaics (PV) result in non-uniform distributions of vacancies[5] which provide regions in which the oxide precipitates can preferentially form. This often results in characteristic concentric rings of poor minority carrier lifetime,[6–8] which can result in very substantial efficiency reductions of order several percent absolute.[6,9] Most photovoltaic solar cells are currently produced from *p*-type silicon substrates, but there is considerable interest in using *n*-type substrates[10,11] as they are generally less susceptible to the

effects of transition metal impurities[12] and do not experience light-induced degradation associated with the boron-oxygen defect.[13] However, oxygen-related extended defects (particularly precipitates and surrounding dislocations and stacking faults) still form in *n*-type Cz-Si.[14] For the development of PV cells in *n*-type silicon, it is important to understand the relationship between oxygen precipitation behaviour and recombination activity, so to understand the impact of a given processing sequence on the final cell efficiency.

Many studies have linked oxygen precipitation in silicon with a reduction in carrier lifetime.[15–24] Recombination at oxide precipitates can arise from both dangling bonds[25,26] and impurities that decorate the precipitates and surrounding extended defects.[20,23,27–29] We have previously published several works on recombination at oxide precipitates in silicon.[21–24,26,29,30] Our work to date has mainly focused on *p*-type silicon. From the analysis of injection-dependent minority carrier lifetime data, we were able to parameterise the recombination activity.[22,24] Our data showed a difference in recombination activity between unstrained and strained oxide precipitates.[21] In samples which were not intentionally contaminated, an approximate correlation between recombination rate and precipitate density was found.[21,22,24] When dislocations and stacking faults were found to surround the precipitates the nature of the recombination centres appeared not to change, but their concentration increased.[22] Recombination in iron-contaminated samples was found to be dependent on the quantity of iron segregated to the precipitates and the precipitate density.[23,24,29] It was shown that in some cases relatively low concentrations of iron could be

a)john.d.murphy@warwick.ac.uk

gettered away from the precipitates by phosphorus diffusion gettering.[24,29]

We have previously published limited data for *n*-type silicon,[22,24] but the lack of a sufficient sample set prevented a detailed study. Motivated by the development of high efficiency PV cells based on *n*-type substrates, in this paper we turn our attention specifically to *n*-type Cz-Si. A set of phosphorus doped samples containing model systems of oxide precipitates has been produced. The approach we used in *p*-type silicon to correlate iron segregation with recombination activity[23,24,29] cannot be applied to our *n*-type material as it relies on photodissociation of FeB pairs to measure the bulk iron concentration. For the *n*-type experiments, we have therefore modified our sample processing to include a polysilicon external gettering layer which is etched away before lifetime measurement. The intention is that relatively fast diffusing metallic impurities are removed from the bulk and hence their possible effects (which are difficult to measure unambiguously) can be neglected. We measure the interstitial oxygen concentration in the samples before and after the oxygen precipitation treatment. By using two distinct types of annealing processes, we are able to create samples containing oxide precipitates with the same densities but with different sizes so we can use this to link recombination activity with precipitate size. As well as providing understanding for the *n*-type case, the oxygen loss correlations provide a useful insight into the mechanism of recombination which is also valid for the *p*-type case.

II. EXPERIMENTAL METHODS

A. Sample preparation

Cz-Si wafers from two *n*-type phosphorus doped 200 mm diameter ingots were first subjected to a *tabula rasa* treatment (1000 °C for 15 min) to dissolve any potential nuclei remaining after the crystallisation process. A poly-silicon external gettering layer was deposited on the rear surface of each wafer by chemical vapour deposition (CVD) at 680 °C for 40 min. For this study, sets of samples were subjected to one of two thermal processes to grow the oxide precipitates:

- Process A ("de-ninja"). This process was designed to produce samples containing only strained precipitates by converting all unstrained precipitates (sometimes called "ninja particles"[4]) into strained ones. The thermal cycle comprised a 4 h anneal at 800 °C, followed by a ∼4 °C/min temperature rise to 925 °C. Wafers were held at 925 °C for 4 h, followed by a ∼4 °C/min temperature rise to 1000 °C. Wafers were held at 1000 °C for 16 h, followed by a 4 °C/min temperature reduction to 800 °C, at which temperature they were unloaded from the furnace.
- Process B ("complex device cycle"). Wafers were subjected to a complex series of thermal cycles designed to simulate an integrated circuit device fabrication process. The full details of the sequence are confidential, but the key point is that each wafer is subjected to multiple (>10) high temperature steps from a baseline temperature of 750 °C. The high temperature steps range from 900 °C to 1175 °C. The key point is that Process B is substantially

different to Process A. It produces samples with similar precipitate densities to Process A but with substantially different sizes. Process B is intentionally not normal for oxide precipitate studies, nor is it similar to a typical solar cell process. Complete conversion of unstrained precipitates into strained ones is unlikely to have occurred in the Process B samples.

After annealing, the poly-silicon gettering layer was etched off the samples using a CP4 etch comprising HF, nitric acid, and acetic acid. The etching process removed material from both sides of the wafers, with the thickness being reduced by $10 \pm 1\ \mu m$ from an initial value of ∼720 μm.

Interstitial oxygen concentrations in all the wafers were measured before and after thermal processing at various locations by infrared absorption measurements. All interstitial oxygen concentrations in this paper are stated to the DIN 50438/I standard. Initial interstitial oxygen concentrations in the centre of the wafers (close to the location of the lifetime samples) were in the range $5.1 \times 10^{17}\ \mathrm{cm^{-3}}$ to $6.8 \times 10^{17}\ \mathrm{cm^{-3}}$. The interstitial oxygen loss after the thermal treatment, $\Delta[O_i]$, was measured in the same position, and this quantity is plotted versus the initial interstitial oxygen concentration in Figure 1(a). A Schimmel etch was used to reveal strained oxide precipitates on cleaved edges of the wafers close to the location of the samples for lifetime measurement. The density of oxide strained precipitates ($N_{strained}$) is plotted against the oxygen concentration loss in Figure 1(b). The data in Figure 1 are discussed later. The doping levels of the samples that underwent Processes A and B were determined from four-point probe measurements to be in the range $1.2 \times 10^{12}\ \mathrm{cm^{-3}}$ to $3.8 \times 10^{13}\ \mathrm{cm^{-3}}$.

B. Surface passivation and lifetime measurement

Samples measuring 5 cm × 5 cm were RCA cleaned prior to surface passivation with ∼70 nm silicon nitride grown on both sides by remote plasma enhanced chemical vapour deposition (PECVD) at approximately 375 °C at ISFH. The lifetime was measured using quasi-steady-state
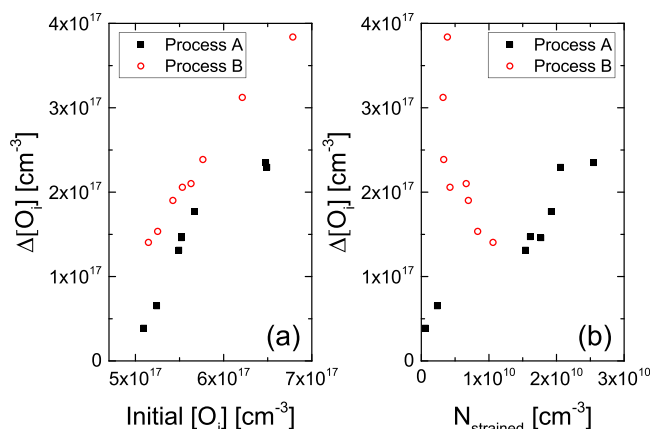

FIG. 1. (a) Initial interstitial oxygen concentration before annealing, $[O_i]$, versus interstitial oxygen loss upon annealing $\Delta[O_i]$. (b) Strained oxide precipitate density determined by chemical etching, $N_{strained}$, versus interstitial oxygen loss upon annealing, $\Delta[O_i]$. Processes A and B display similar trends in (a) but not in (b).

photoconductance (QSS-PC)[31] or transient photoconductance decay using a Sinton WCT-120 lifetime tester. The measured lifetime (τ_{measured}) is corrected to give the residual lifetime (τ_{residual}) defined according to

$$\tau_{\text{residual}} = \left(\frac{1}{\tau_{\text{measured}}} - \frac{1}{\tau_{\text{intrinsic}}} \right)^{-1}, \quad (1)$$

where τ_{residual} is the lifetime due to intrinsic recombination processes (Auger and band-to-band). In this paper, the parameterisation used for intrinsic recombination is that of Richter *et al.*[32] This is different to that used in our previous work[21–24,29] as the studies were started before this more accurate parameterisation was available. For most cases considered here this change is negligible. Control samples (from the same ingots but without oxygen precipitation treatments) were used to estimate the efficacy of the surface passivation treatment, as discussed later.

C. Analysis of injection-dependent lifetime data

To analyse the injection-dependent minority carrier lifetime data, we use a linear formulation of Shockley-Read-Hall (SRH) statistics, which we have described in detail previously.[22] In *n*-type material, the hole lifetime associated with a single SRH defect varies according to

$$\tau_p = \frac{1}{\alpha_p N} \left[1 + \frac{n_1}{n_0} + \frac{p_1}{n_0 Q} + Y \left(\frac{1}{Q} - \frac{n_1}{n_0} - \frac{p_1}{Q n_0} \right) \right], \quad (2)$$

where the hole and electron concentrations (denoted by p and n, respectively) are entirely included in $Y = \frac{p}{n}$. The SRH densities, n_1 and p_1, are defined according to

$$n_1 = N_C \exp \left(-\frac{(E_C - E_T)}{kT} \right), \quad (3)$$

$$p_1 = N_V \exp \left(-\frac{(E_T - E_V)}{kT} \right), \quad (4)$$

where N_C and N_V are the density of states in the conduction and valence bands, respectively, and E_T is the energy level of the defect. The remaining variables in Equation (1) are the capture coefficient for holes (α_p), the equilibrium electron concentration (n_0), and the asymmetry factor ($Q = \frac{\alpha_n}{\alpha_p}$, where α_n is the capture coefficient for electrons).
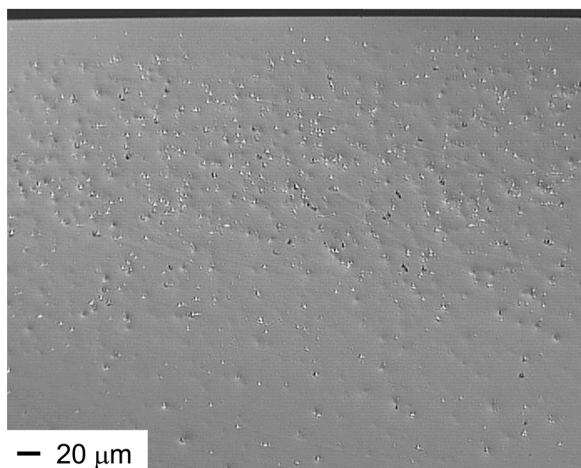
Our previous work based mainly upon *p*-type silicon found that recombination at oxide precipitates could be described in terms of two independent SRH centres.[22,24] The physical origin of these centres is not confirmed, so we refer to them simply as "Defect 1" and "Defect 2." The residual hole lifetime in *n*-type silicon containing two independent SRH centres can be written as

$$\tau_{\text{residual}} = \left[\left(\frac{1}{\alpha_{p1} N_1} \left[1 + \frac{n_1}{n_0} + \frac{p_1}{n_0 Q_1} + Y \left(\frac{1}{Q_1} - \frac{n_1}{n_0} - \frac{p_1}{Q_1 n_0} \right) \right] \right)^{-1} + \left(\frac{1}{\alpha_{p2} N_2} \left[1 + \frac{n_2}{n_0} + \frac{p_2}{n_0 Q_2} + Y \left(\frac{1}{Q_2} - \frac{n_2}{n_0} - \frac{p_2}{Q_2 n_0} \right) \right] \right)^{-1} \right]^{-1}, \quad (5)$$

where the numerical subscripts indicate the parameters relating to Defects 1 and 2, respectively. For oxide precipitates, we previously determined that E_1 lies at $E_V + 0.22\,\text{eV}$ and $E_2 = E_C - 0.08\,\text{eV}$, and that $Q_1 = 157$ and $1/Q_2 = 1200$ at room temperature.[22] Equation (5) is used with these parameters to fit the injection-dependent lifetime data in the *n*-type case.

III. RESULTS AND ANALYSIS

A. Oxygen losses and precipitate densities

The aim of this study is not to conduct a detailed investigation of oxygen precipitation nucleation and growth kinetics as such studies have been performed before (e.g., Ref. 33). Data relating to the precipitation process have been acquired insofar as they are necessary to support the carrier lifetime study. Figure 1(a) is a plot of the starting interstitial oxygen concentration versus interstitial oxygen lost from the bulk during the thermal annealing process. For both Process A and Process B, the oxygen loss is dependent on the initial interstitial oxygen concentration, as expected from classical precipitation nucleation and growth theories.[33,34] Figure 1(b) is a plot of strained oxide precipitate density determined by chemical etching versus the interstitial oxygen lost from the

bulk during the precipitation process. For Process A, this trend is approximately linear. The average number of oxygen atoms in each strained precipitate is approximately constant, and this average does not appear to vary significantly with the total amount of oxygen lost. We cannot rule out the possibility that there are a wide spread of sizes, but on average the precipitates in the Process A samples are approximately the same size. For Process B, samples with a higher initial interstitial oxygen concentration have a substantially higher oxygen loss than samples with lower initial interstitial oxygen concentrations. Comparison of Figure 1(a) with Figure 1(b) indicates that fewer strained precipitates are formed in the Process B samples with the higher initial interstitial oxygen concentrations than in those with lower interstitial oxygen concentrations.

Figure 1(b) demonstrates that the onset of observable precipitates (by etching) occurs with very small changes of interstitial oxygen concentration (i.e., the plot almost goes through the origin). This shows that Process A (the "de-ninja" cycle) achieved its aim of converting most unstrained precipitates into strained precipitates. This means that to a good approximation, we can consider the Process A samples to contain only strained oxide precipitates.

For Process B samples, Figure 1(b) shows relatively high oxygen losses for small densities of strained oxide precipitates. Based on oxygen loss data alone, one explanation for this could be that more oxygen in the Process B samples is in the form of unstrained precipitates (not detectable by etching). However, there is also evidence for the strained precipitates in the Process B samples being larger than those in the Process A samples. Evidence comes from an optical microscopy investigation of the etch pits on cross-sectioned samples. Figure 2 shows etched samples with a similar density of strained oxide precipitates from (a) Process A and (b) Process B. Many of the etch pits in the Process B sample are elongated ($>10\,\mu m$ in length), whereas in the Process A sample they are mainly circular. Elongated etch pits such as these are known to result from stacking faults,[35] and these form when the oxide precipitates grow above a critical size.[3,4,36] Similar behaviour was found in all other Process B samples studied, with such etch pits not being observed in significant concentrations in any of the Process A samples. We therefore conclude that in samples with a low density of oxide precipitates, the precipitates are larger in Process B samples than in Process A samples.

B. Intrinsic and surface recombination effects

Figure 3 shows the measured lifetime in a control sample from the same ingot which was not subjected to an oxygen precipitation treatment, but which underwent the same surface passivation as those which were processed to containing oxide precipitates. The measured lifetime (τ_{measured}), residual lifetime (τ_{residual}) according to Equation (1), and the intrinsic lifetime ($\tau_{\text{intrinsic}}$) according to Richter *et al.*[32] are plotted. It is noted that the lifetime correction of Richter *et al.* has a very small impact on the measured lifetime, even for this control sample which has a very high bulk lifetime in the millisecond range. The inset of Figure 3 shows the upper limit of the surface recombination velocity (S), calculated assuming an infinite bulk lifetime using $S = \frac{W}{2\tau_{\text{residual}}}$, where τ_{residual} is defined by Equation (1) and W is the sample thickness. The upper limit of the surface recombination velocity is below $10\,\text{cm s}^{-1}$ for $X = n/p < 0.9$. At higher injection levels, the upper limit of the surface recombination velocity increases to a maximum of $26\,\text{cm s}^{-1}$ at $X = n/p = 0.992$.

If it is assumed the bulk lifetime is infinite, τ_{residual} for the control sample in Figure 3 represents the lifetime due to recombination at the sample surfaces under the passivation scheme used. Figure 4 shows the measured lifetime in samples containing oxide precipitates, and the corresponding residual lifetime and the residual lifetime from which surface recombination as quantified from Figure 3 have also been subtracted ($\tau_{\text{residual + surface}}$). Figure 4 shows that the correction due to intrinsic recombination is very small. It also shows that any surface recombination effect is very small for the low lifetime sample shown. In the higher lifetime sample shown, the effect of the surfaces on lifetime is still small,

(a) Process A $N_{\text{strained}} = 2.4 \times 10^9\ \text{cm}^{-3}$
$\Delta[O_i] = 6.5 \times 10^{16}\ \text{cm}^{-3}$

— 20 μm

(b) Process B $N_{\text{strained}} = 3.9 \times 10^9\ \text{cm}^{-3}$
$\Delta[O_i] = 3.8 \times 10^{17}\ \text{cm}^{-3}$
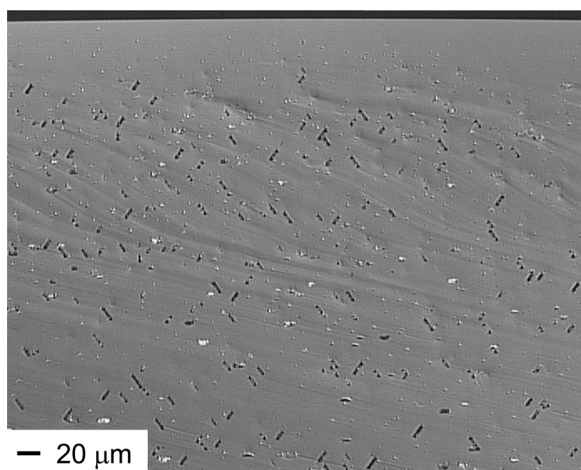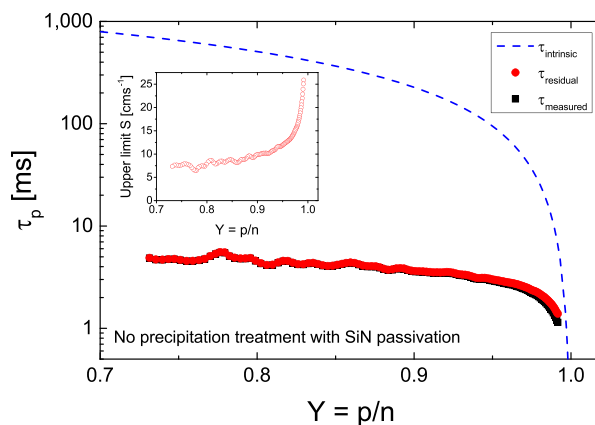

— 20 μm

FIG. 2. Optical micrographs of etched cross-sections of representative samples from (a) Process A and (b) Process B, with the sample surface at the top of the images. Extended etch channel characteristics of stacking faults appear in the Process B sample, but not in the Process A sample. Lifetime data from these wafers are presented in Figure 7.

FIG. 3. Minority carrier lifetime in a 720 μm thick *n*-type Cz-Si control sample with a phosphorus doping level of $7 \times 10^{13}\ \text{cm}^{-3}$ which was not annealed but underwent the same cleaning and silicon nitride surface passivation processes at the oxide precipitate-containing samples. The intrinsic lifetime ($\tau_{\text{intrinsic}}$) was factored out of the measured lifetime (τ_{measured}) to give the residual lifetime (τ_{residual}) according to Equation (1). The inset shows the upper limit of the surface recombination velocity (S), calculated as described in the text.
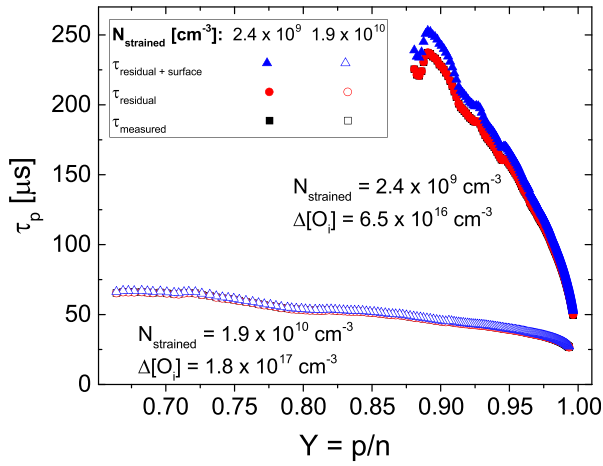
FIG. 4. Measured minority carrier lifetime ($\tau_{measured}$), residual lifetime according to Equation (1) ($\tau_{residual}$), and the residual lifetime empirically corrected for surface recombination using the data in Figure 3 ($\tau_{residual+surface}$) for two *n*-type Cz-Si samples with a phosphorus doping level of 3×10^{13} cm^{-3} containing oxide precipitates produced by Process A.

with the difference between $\tau_{residual\ +\ surface}$ and $\tau_{residual}$ just ~6.5% at $X = n/p = 0.9$.

It is noted that the samples in Figures 3 and 4 have fairly similar doping levels. It is however likely that the surface recombination is dependent on the majority carrier concentration.[37] Control samples with substantially different doping levels from the same ingots were not available, so rather than factor out the surface recombination effects from the parameterisation it was decided instead to regard them as negligible. Figure 4 confirms that this is a reasonable assumption for the samples for which results are presented here.

C. Injection-dependent lifetime results

Figure 5 shows the residual minority carrier lifetime in *n*-type samples containing oxide precipitates produced by Process A. The data are grouped into two separate plots, with Figure 5(a) showing those for samples with a "medium" level of phosphorus doping ($3.3 \pm 0.3 \times 10^{13}$ cm^{-3}) and Figure 5(b) showing those for samples with a "low" level of

phosphorus doping ($1.8 \pm 0.9 \times 10^{12}$ cm^{-3}). The trend in both plots is for the lifetime to reduce with increasing oxide precipitate density and increasing interstitial oxygen loss. The dependence of lifetime on these two variables is discussed in detail later.

Figure 6 shows the residual minority carrier lifetime in *n*-type samples with substantially different doping levels, but with very similar measured oxide precipitate densities and interstitial oxygen losses. The low and medium doped samples were subjected to Process A. Also shown in Figure 6 is a curve for a high-doped sample (8.4×10^{14} cm^{-3}) from a previous study[22] which is included to demonstrate more clearly the effect of the variation of doping level. This sample underwent an oxygen precipitation process similar to Process A (full details given in Ref. 21), although without the "de-ninja" step to ensure full conversion to strained precipitates. The unstrained precipitates are not strong recombination centres,[21] and empirically the data from the samples are found to be consistent. The injection-dependence of the residual lifetime varies substantially between the three samples. This behaviour can be explained by the parameterisation of the recombination activity in terms of two SRH centres. The experimental data in Figure 6 have been fitted using the parameterisation stated in Section II C, with only the two $N\alpha_p$ "recombination parameters" as independent variables. As shown in the legend of Figure 6, similar values of $N_1\alpha_{p1}$ and $N_2\alpha_{p2}$ are used for all three datasets. The difference in the lifetime behaviour therefore principally arises from dependence of certain terms in Equation (5) on n_0.

Figure 7 shows the residual lifetime in two samples with medium doping level, with one sample subjected to Process A and the other to Process B. For the data shown, the strained precipitate densities are quite similar (2.4×10^9 cm^{-3} and 3.9×10^9 cm^{-3}, respectively), but the oxygen losses which occur during processing are substantially different (6.5×10^{16} cm^{-3} and 3.8×10^{17} cm^{-3}). The optical micrographs in Figure 2 come from the same wafers as the lifetime data in Figure 7,
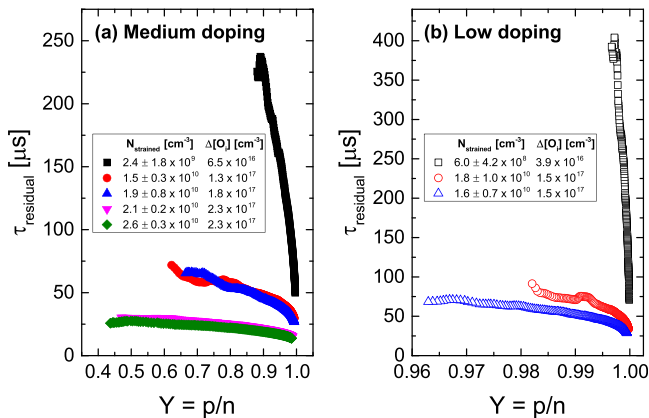

FIG. 5. Residual lifetime in *n*-type samples subjected to Process A. Measured precipitate densities and the interstitial oxygen losses are indicated in the legend. Graph (a) shows data from "medium" doped samples containing $3.3 \pm 0.3 \times 10^{13}$ cm^{-3} of phosphorus. Graph (b) shows data from "low" doped samples containing $1.8 \pm 0.9 \times 10^{12}$ cm^{-3} of phosphorus.
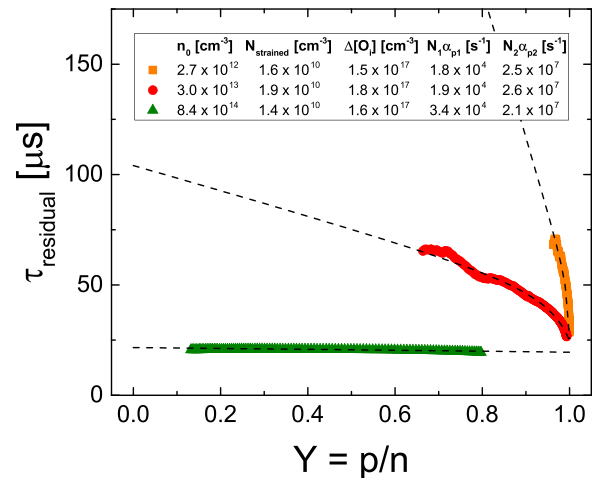
FIG. 6. Residual minority carrier lifetime versus $Y = p/n$ for three *n*-type Cz-Si samples with substantially different doping levels ("low," "medium," and "high"), but with very similar strained oxide precipitate densities ($N_{strained}$) and interstitial oxygen losses ($\Delta[O_i]$). The dashed lines are fits to the experimental data using Equation (5) and the previously published parameterisation[22] using the fit parameters stated in the legend.
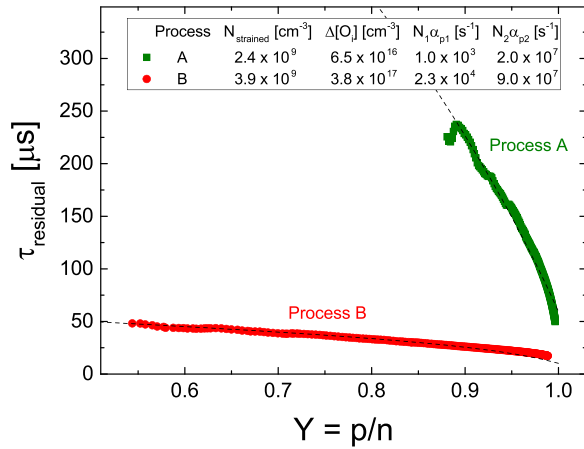
Process	$N_{strained}$ [cm^{-3}]	Δ[O] [cm^{-3}]	$N_1\alpha_{p1}$ [s^{-1}]	$N_2\alpha_{p2}$ [s^{-1}]
A	2.4×10^9	6.5×10^{16}	1.0×10^3	2.0×10^7
B	3.9×10^9	3.8×10^{17}	2.3×10^4	9.0×10^7

FIG. 7. Residual lifetime in two samples with a doping level of 3×10^{13} cm^{-3} which have a similar density of strained oxide precipitates arrived at by very different processes. The sample subjected to Process B has a much larger bulk oxygen loss than the Process A sample.

and the stacking faults observed in the Process B sample indicate that its precipitates are much larger. The injection-dependent data can be fitted using the standard parameterisation, with the fit parameters stated in the legend. Although the Process B sample has a slightly higher precipitate density than the Process A sample, this alone cannot explain the different recombination parameters measured. The difference in behaviours can be accounted for by considering the relative average precipitate sizes, as detailed in Section III D.

D. Analysis in terms of precipitate morphologies

The data presented in Figure 5 show that the recombination rate is dependent, in some way, upon the density of strained oxide precipitates. However, the data in Figure 7 show that the precipitate density is not the only factor which determines the recombination activity. Possible origins of recombination in our samples include:

(i)   Processes dependent only upon the density of oxide precipitates. We have previously suggested the possibility of the recombination arising from a feature of the precipitates which is invariant with size (such as corners),[21,26] having ruled out the possibility of diffusion-limited capture.[38]

(ii)   Interface-related recombination whereby recombination centres are dispersed at the SiO$_2$-Si interface. This could be the P_{b0} or P_{b1} dangling bond centres which have been shown to exist in oxide precipitate-containing silicon.[25,26]

(iii)   Impurity-related recombination whereby impurities, such as transition metals, decorate precipitates, and surrounding extended defects.[20,23,27–29] Evaluation of the role of very low impurity concentrations is very challenging, and our assumption is that the external polysilicon-based gettering procedure removes the impurities from the material.

The lifetime data can be analysed in conjunction with the oxygen loss data to ascertain whether the recombination activity arises due to (i) density-dependent or (ii) interface

area-dependent centres. Fitting the lifetime data with the SRH parameterisation requires two fit parameters ($N_1\alpha_{p1}$ and $N_2\alpha_{p2}$), which are the product of a state density and a capture coefficient for holes at associated with that defect. On the assumption that the capture coefficients are invariant, these fit parameters are directly proportional to the density of recombination centres. Correlation of the fit parameters with strained precipitate density from etching is trivial. Calculating the interface area from oxygen loss measurements requires assumptions to be made about the precipitate morphology and the relative recombination strength of strained and unstrained oxide precipitates. It is also required that the stacking faults around the oxide precipitates are electrically inactive. This is a reasonable assumption supported by previous work in *n*-type silicon that has shown stacking faults not to be recombination active.[39]

In general, the total interstitial oxygen loss measured by infrared absorption experiments (Δ[O$_i$]) goes to oxide precipitates of both unstrained and strained types, that is

$$\Delta[\text{O}_i] = [\text{O}_{\text{strained}}] + [\text{O}_{\text{unstrained}}], \qquad (6)$$

where [O$_{\text{strained}}$] and [O$_{\text{unstrained}}$] are the oxygen concentrations lost to strained and unstrained oxide precipitates, respectively. Our previous work has indicated that unstrained oxide precipitates are much less recombination active than strained oxide precipitates.[21] For the purposes of this analysis, it is therefore assumed that recombination at the unstrained precipitates is negligible compared to that at the strained precipitates. Unfortunately, we are unable to measure [O$_{\text{strained}}$] directly though, as the infrared absorption measurements give Δ[O$_i$], which according to Equation (6) includes a contribution from [O$_{\text{unstrained}}$]. In the special case of Process A, a near complete conversion into strained precipitates has occurred, and so we can assume Δ[O$_i$] $\approx$ [O$_{\text{strained}}$] for this sample set. This assumption is not valid for Process B.

The average volume of a single strained oxide precipitate (v) relates to [O$_{\text{strained}}$] and the precipitate number density (N_{strained}) according to

$$v = \frac{[\text{O}_{\text{strained}}]}{\rho N_{\text{strained}}}, \qquad (7)$$

where ρ is the average *atomic* density of the silicon dioxide precipitates.

As a first approximation, the strained oxide precipitates could be treated as spheres,[36] with radius r and volume $v = \frac{4}{3}\pi r^3$. Using Equation (7), the radius of a single spherical strained oxide precipitate is

$$r = \left(\frac{3[\text{O}_{\text{strained}}]}{4\pi\rho N_{\text{strained}}}\right)^{\frac{1}{3}}. \qquad (8)$$

The surface area of a single spherical oxide precipitate, a_{sphere}, is given by

$$a_{\text{sphere}} = 4\pi r^2 = 4\pi\left(\frac{3[\text{O}_{\text{strained}}]}{4\pi\rho N_{\text{strained}}}\right)^{\frac{2}{3}}. \qquad (9)$$

It follows that the total surface area of the precipitates in unit volume, A_{spheres}, is given by

$$A_{\text{spheres}} = N_{\text{strained}} a_{\text{sphere}} = (4\pi N_{\text{strained}})^{\frac{1}{3}} \left(\frac{3[\text{O}_{\text{strained}}]}{\rho} \right)^{\frac{2}{3}}. \quad (10)$$

Equations (10) and (6) can be used to express the $N_i\alpha_{pi}$ recombination parameters due to two SRH recombination centres distributed around the surface of the spherical strained precipitates as

$$N_i\alpha_{pi} = \eta_i\alpha_{pi}(4\pi N_{\text{strained}})^{\frac{1}{3}} \left(\frac{3\left(\Delta[\text{O}_i] - [\text{O}_{\text{unstrained}}]\right)}{\rho} \right)^{\frac{2}{3}}, \quad (11)$$

where $i = 1$ for Defect 1 and $i = 2$ for Defect 2, and η_i is the density of the ith recombination centre per unit surface area of the precipitates. In the special case that all the lost oxygen ends up in strained precipitates, the recombination parameters in the spherical precipitate case are both proportional to $N_{\text{strained}}^{\frac{1}{3}}\Delta[\text{O}_i]^{\frac{2}{3}}$.

Alternatively, oxide precipitates can be thin square plates.[40] The volume of one such precipitate is $l^2 d$, where l is the length of the sides of the square and d is the thickness. From Equation (7)

$$l = \sqrt{\frac{[\text{O}_{\text{strained}}]}{\rho N_{\text{strained}} d}}. \quad (12)$$

Under the assumption that $l \gg d$ (justified by experimental studies in the literature[3,40]), the surface area of a single platelet is given by

$$a_{\text{platelet}} = 2l^2 = \frac{2[\text{O}_{\text{strained}}]}{\rho N_{\text{strained}} d}. \quad (13)$$

The total surface area of the strained platelets in a unit volume, $A_{\text{platelets}}$, is therefore

$$A_{\text{platelets}} = N_{\text{strained}} a_{\text{platelet}} = \frac{2[\text{O}_{\text{strained}}]}{\rho d}. \quad (14)$$

Equations (14) and (6) can be used to express the $N_i\alpha_{pi}$ recombination parameters due to two SRH recombination centres distributed around the large area surfaces of the strained platelets as

$$N_i\alpha_{pi} = \eta_i'\alpha_{pi}\frac{2}{\rho d}\left(\Delta[\text{O}_i] - [\text{O}_{\text{unstrained}}]\right), \quad (15)$$

where $i = 1$ for Defect 1 and $i = 2$ for Defect 2, and η_i' is the density of the ith recombination centre per unit surface area of the platelet precipitates. In the special case that all the lost oxygen ends up in strained precipitates, the recombination parameters in the platelet case are both proportional to $\Delta[\text{O}_i]$.

Figure 8 shows plots of the recombination parameters ($N_1\alpha_{p1}$ and $N_2\alpha_{p2}$) versus (a) N_{strained}, (b) $N_{\text{strained}}^{\frac{1}{3}}\Delta[\text{O}_i]^{\frac{2}{3}}$, and (c) $\Delta[\text{O}_i]$ for Process A samples. In all cases the correlation is approximately linear. It is noted that as the plots for any one of the three variables are linear, it is not surprising that the plots for both other variables are also linear given the approximate linear relationship between N_{strained} and $\Delta[\text{O}_i]$ demonstrated for Process A in Figure 1(b).

Figure 9 show plots of the recombination parameters ($N_1\alpha_{p1}$ and $N_2\alpha_{p2}$) versus (a) N_{strained}, (b) $N_{\text{strained}}^{\frac{1}{3}}\Delta[\text{O}_i]^{\frac{2}{3}}$, and (c) $\Delta[\text{O}_i]$ for samples which have undergone Process B, respectively. Process B is likely to have created both unstrained and strained oxide precipitates; therefore, the approximation $\Delta[\text{O}_i] \approx [\text{O}_{\text{strained}}]$ does not hold. Figure 9(a) shows no apparent correlation between the recombination parameters and N_{strained} for the Process B samples. For samples containing both unstrained and strained precipitates, Equation (15) predicts a linear correlation of the recombination parameters with $\Delta[\text{O}_i]$ in the case of platelets with the intercept with the recombination parameter axis occurring below the origin. The Figure 9(c) graphs show that the experimental data do not agree with this prediction. Figure 9(b) for the case of spherical precipitates does show a correlation for Process B samples and this is discussed later.

IV. DISCUSSION

A. Parameterisation

One of the aims of this study was to quantify minority carrier lifetime in n-type silicon. As control samples from the same ingots were available, we quantified the effect of any remaining surface recombination on the minority carrier lifetime. The passivation scheme used was shown to provide a very low surface recombination velocity (Figure 3). Figure 4 shows data from which the surface-related recombination has been subtracted. The effect of surface recombination can be seen to be very small. We have chosen not to try to factor out surface recombination from our parameterisation of oxide precipitate-related recombination as the effect is small and the surface recombination would probably also be dependent on the doping level.

Figure 6 clearly demonstrates the dependence of the majority carrier concentration on the injection-dependent minority carrier lifetime, as the samples considered have very similar oxide precipitate densities and bulk oxygen losses upon precipitation. The data can be fitted using Equation (5) with our previously published parameterisation and similar $N_1\alpha_{p1}$ and $N_2\alpha_{p2}$ recombination parameters. This confirms the applicability of our two defect SRH approach[22,24] for parameterisation of recombination in oxide precipitate-containing silicon for both doping types.

To minimise surface recombination, the samples studied here and previously[21–24,26,29,30] were passivated prior to lifetime measurement with a silicon nitride film grown by PECVD. This layer is hydrogen rich and some of this hydrogen may diffuse into the bulk. Prior work using deuterated silicon nitride fired at $800\,^{\circ}\text{C}$ (considerably higher than our deposition temperature of approximately $375\,^{\circ}\text{C}$) has provided evidence for deuterium trapping at oxide precipitates.[41] Even at the relatively low temperatures we use, it is possible that hydrogen can diffuse into the bulk of the material. It is possible, although not proven, that such bulk hydrogen (if present) could passivate some of the recombination activity associated with oxide precipitates. It is noted that our parameterisation has only been tested for silicon nitride passivated samples, but this is likely to be appropriate for
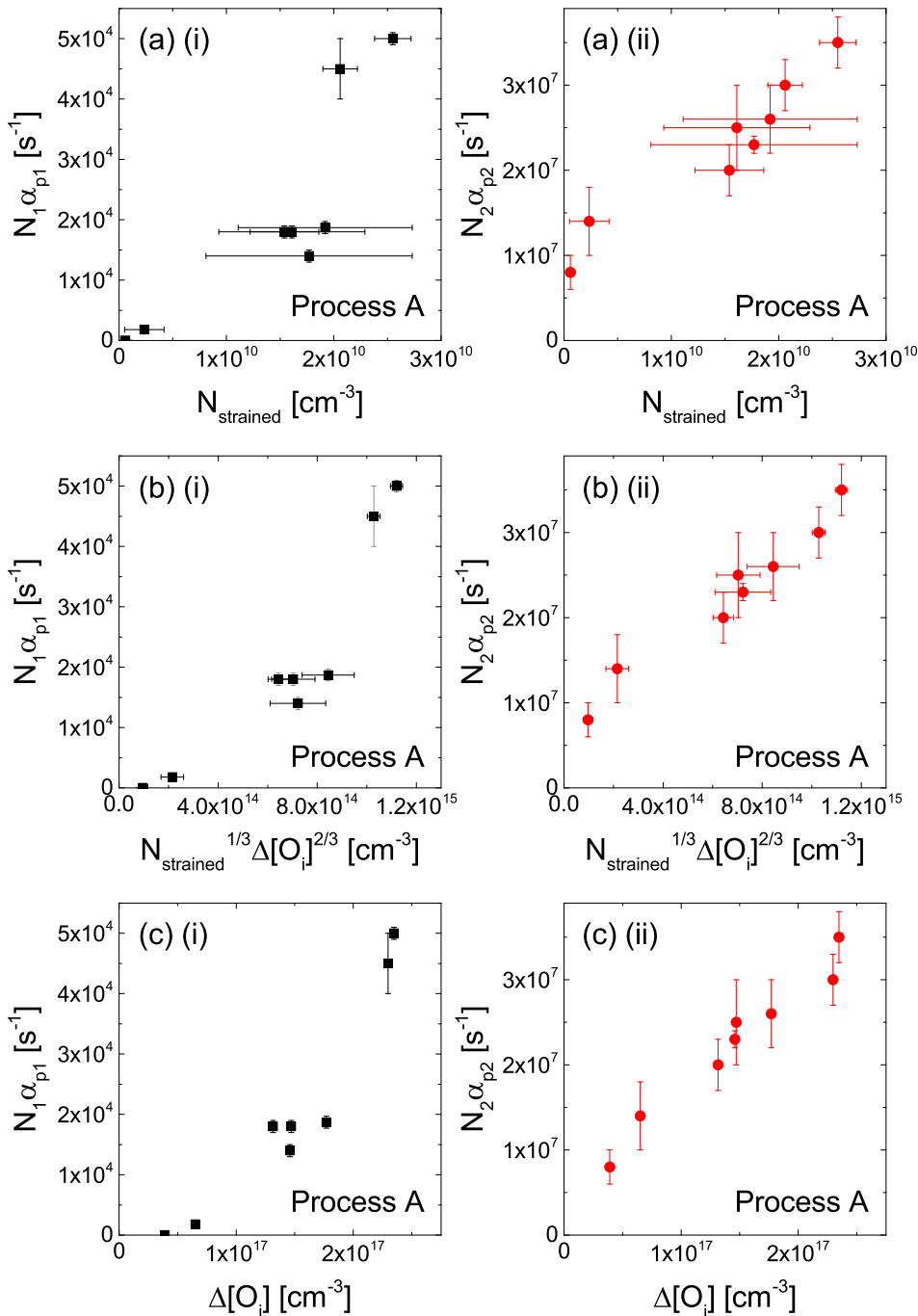
FIG. 8. Plots of recombination parameters (i) $N_1\alpha_{p1}$ for Defect 1 and (ii) $N_2\alpha_{p2}$ for Defect 2 for *n*-type Cz-Si samples subjected to Process A versus: (a) strained oxide precipitate density ($N_{strained}$); (b) $N_{strained}^{\frac{1}{3}}\Delta[O_i]^{\frac{2}{3}}$ to test for spherical precipitates according to Equation (11); and (c) $\Delta[O_i]$ to test for platelet precipitates according to Equation (15).

B. Size versus density dependence

In order to apply the parameterisation of minority carrier lifetime in *n*-type silicon, it is necessary to know how the $N_1\alpha_{p1}$ and $N_2\alpha_{p2}$ recombination parameters relate to a measurable property of the precipitates. Using lifetime measurements alone, it is not possible unambiguously to separate the density terms (N_1 and N_2) from the hole capture coefficient terms (α_{p1} and α_{p2}), but we assume an invariance of the capture coefficients so that the recombination parameters are proportional to the state density.

most solar cell materials to which a silicon nitride layer is often applied for surface passivation and to act as an anti-reflection coating.

Our previous work in *p*-type silicon found a correlation between the recombination parameters and the density of strained precipitates from etching.[22,24] We knew from prior TEM studies that the precipitates in the *p*-type samples had very different sizes ranging from largest dimensions of 30–50 nm to ~500 nm.[4] We did not have IR interstitial oxygen loss data available for each sample, so we were unable to correlate recombination parameters with precipitate surface area parameters as we have done here. From a supporting TEM study, we were able to determine that surrounding dislocations and stacking faults increased the recombination activity by a factor of 3–4 in the *p*-type samples studied,[21] but the increase was due to an increased concentration of the same recombination centres.[22] So, while in our previous works there appeared to be an approximate correlation
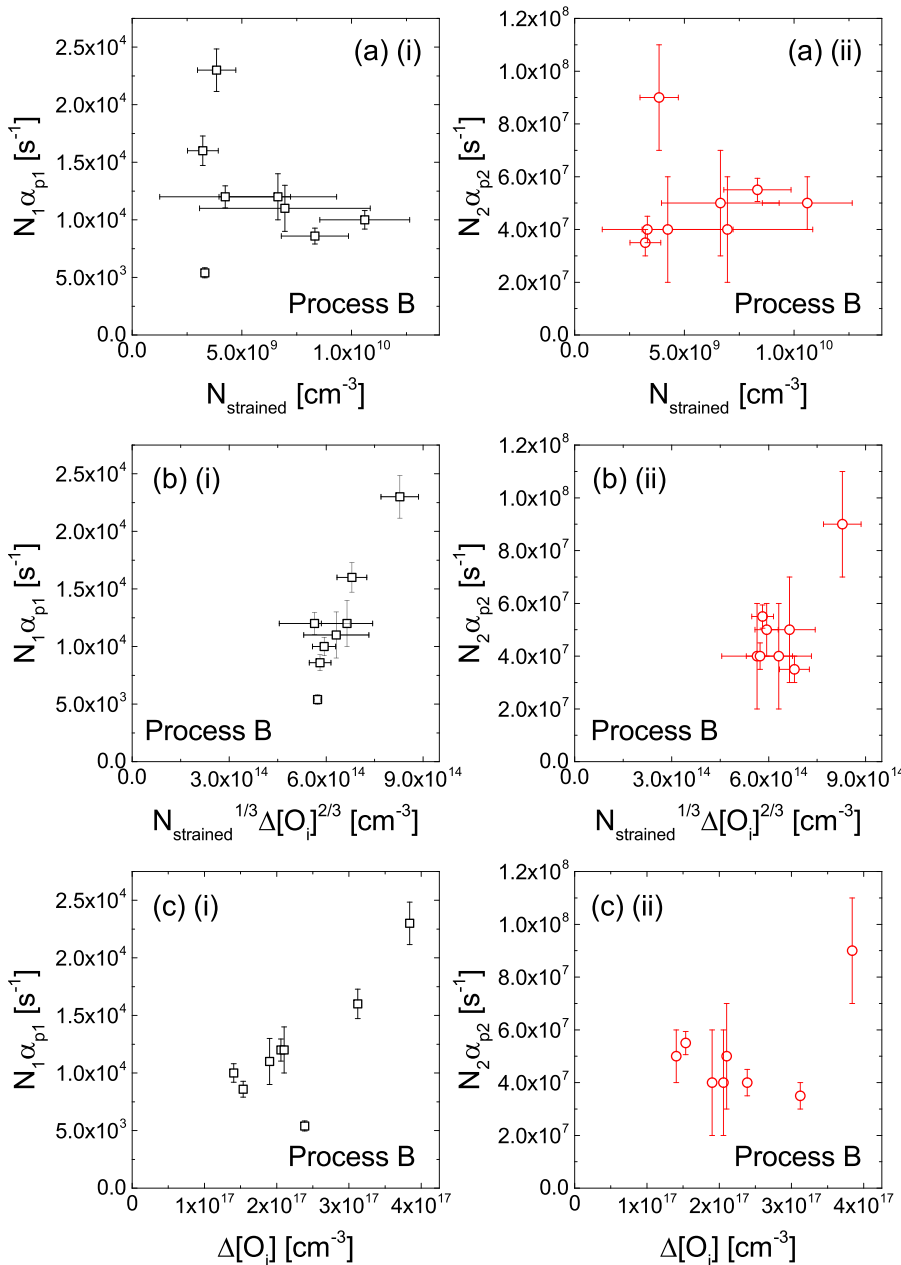
FIG. 9. Plots of recombination parameters (i) $N_1\alpha_{p1}$ for Defect 1 and (ii) $N_2\alpha_{p2}$ for Defect 2 for *n*-type Cz-Si samples subjected to Process B versus: (a) strained oxide precipitate density (N_{strained}); (b) $N_{\mathrm{strained}}^{\frac{1}{3}}\Delta[\mathrm{O}_i]^{\frac{2}{3}}$ to test for spherical precipitates according to Equation (11); and (c) $\Delta[\mathrm{O}_i]$ to test for platelet precipitates according to Equation (15).

between oxide precipitate density and the recombination parameters, this correlation could have been coincidental. The increased recombination in samples in which stacking faults and dislocations surrounded the precipitates could be explained by larger precipitates with more surface area giving rise to more of the same type of recombination. The possibility that recombination arises due to centres proportional to the interface area of the precipitates is not excluded by our previously published data.

In samples subjected to the de-ninja process (Process A), Figure 1(b) shows that there is approximately linear correlation between the oxygen loss and the density of strained precipitates. Unsurprisingly therefore, the correlations in Figure 8 do not allow us to resolve the density-surface area debate. Figure 9, which contains data from the Process B samples, does provide a useful insight into the origin of the recombination centres however. Figure 9(a) shows that there is no simple correlation between $N_1\alpha_{p1}$ or $N_2\alpha_{p2}$ and N_{strained}.

This demonstrates that our density argument, in which we suggested recombination occurs at a feature of the precipitates invariant with size (such as corners), is not likely to apply in this case.

We now consider the possibility of interface-dependent recombination in the Process B samples. Figure 9(b) aims to test the correlation for strained spherical precipitates, according to Equation (11) and Figure 9(c) aims to test for strained platelets. In the case of platelet precipitates, Equation (15) predicts a linear correlation in Figure 9(c) with a vertical axis intercept below the origin due to the unstrained precipitates in the Process B samples. The correlation shown in Figure 9(c) is clearly better than in Figure 9(a), particularly in the case of Defect 1, but there are some outlying points and the correlation for Defect 2 is not particularly convincing. The best correlation is found in Figure 9(b). It is noted that Equation (11) includes an unknown $[\mathrm{O}_{\mathrm{unstrained}}]$ term. This explains why the correlations in Figure 9(b) can be

extrapolated to vertical axis intercept below the origin. It is not possible to extract a single value for $[O_{unstrained}]$ for the Process B samples, as the value in each sample will be different due to the different initial interstitial oxygen concentrations.[4] The data in Figure 9 therefore suggest that recombination in oxide precipitate-containing silicon is dependent on the interface area and not precipitate density as we have assumed until now.

An issue which needs resolving is the role of impurities in the recombination mechanism. We have shown previously in p-type silicon that iron segregation to the oxide precipitates and surrounding defects appears to increase the density of the same recombination centres[23,24,29] as those found here in the n-type samples. One possibility is that the recombination activity arises from impurities residing at available sites whose density depends upon precipitate surface area. Such impurities would need to be strongly bound to these sites, so as not to be externally gettered. Another possibility is that recombination arises from P_{b0} and P_{b1} dangling bonds, which have been shown in spin resonance experiments to be associated with oxygen precipitation.[25,26] It is reasonable to expect that the density of dangling bonds depends upon interface area, but a problem with this explanation is that dangling bonds can be hydrogen passivated[25,42] and this may well have occurred during the silicon nitride surface passivation process. The precise details of the recombination mechanism are a matter of active research.

C. Interface recombination velocities

Our data suggest a correlation between recombination activity and precipitate surface area. The $\eta_i\alpha_{pi}$ parameters in Equation (11) can be regarded as recombination velocities at the interface between the bulk silicon and the oxide precipitates. For Process A, $[O_{unstrained}]$ is negligible, so under the assumption of spherical precipitates, the gradient of the plots in Figure 8(b) can be used to estimate the $\eta\alpha_p$ parameters, with the gradients of the plots being equal to $\eta_1\alpha_{p1}(4\pi)^{\frac{1}{3}}(\frac{3}{\rho})^{\frac{2}{3}}$ or $\eta_2\alpha_{p2}(4\pi)^{\frac{1}{3}}(\frac{3}{\rho})^{\frac{2}{3}}$. The gradient for Defect 1 is of order $3 \times 10^{-11}\,cm^3\,s^{-1}$ and the gradient for Defect 2 is of order $3 \times 10^{-8}\,cm^3\,s^{-1}$. Taking a value of ρ from Newman *et al.* as $4.5 \times 10^{22}\,cm^{-3}$ (Ref. 43) gives $\eta_1\alpha_{p1} \approx 8 \times 10^3\,cm\,s^{-1}$ and $\eta_2\alpha_{p2} \approx 8 \times 10^6\,cm\,s^{-1}$ for Process A.

Our $\eta\alpha_p$ parameters can be compared to the oxide precipitate surface recombination velocity parameters of Hwang and Schroder, which are of order $10^4\,cm\,s^{-1}$ to $10^5\,cm\,s^{-1}$.[18] Hwang and Schroder determined lifetimes with a surface photovoltage techniques which operates at low levels of carrier injection. Measured minority carrier lifetimes in this regime will have been dominated by our Defect 1, which is why most of their data have surface recombination velocities between our two values, but closer to that for Defect 1 than that for Defect 2. Our recombination velocity data are therefore consistent with those of Hwang and Schroder, who did not consider a two defect approach.

It is also worth noting that Sio *et al.* have recently measured recombination velocities at grain boundaries in multicrystalline silicon (mc-Si) for photovoltaics.[44] Our recombination values for oxide precipitates are, in general, much higher than

theirs for grain boundaries in as-received samples which are often $<2000\,cm\,s^{-1}$. While they do measure recombination velocities similar to our Defect 1 values in gettered mc-Si from the middle of the block, our Defect 2 recombination velocity is substantially higher than any they measure associated with grain boundaries. This suggests that, per unit area, the interfaces between oxide precipitates and the silicon bulk are probably more recombination active than metal decorated grain boundaries.

D. Recombination in *n*-type versus *p*-type silicon

The vast majority of silicon photovoltaic cells are fabricated from p-type substrates, although n-type substrates may enable the production of higher efficiency cells.[10,11] Oxide precipitates are likely to form in rapidly pulled silicon, regardless of doping type, so it is important to understand their relative impact on lifetime. Hwang and Schroder concluded that oxide precipitates are more detrimental to minority carrier lifetime in p-type silicon than in n-type silicon.[18] However, as discussed above, their surface photovoltage measurements were made at low injection and hence this conclusion about doping type and lifetime is only valid at relatively low excess carrier concentrations (below the typical operating conditions of a photovoltaic cell). We have previously published a comparison of lifetime in n-type versus p-type silicon,[24] but with the new oxygen loss results presented here we have been able to relate the precipitate surface area to state density.

In n-type silicon, we have demonstrated a probable correlation between precipitate surface area and a term proportional to the density of recombination states. We have also shown that the lifetime in both n-type and p-type silicon can be parameterised in terms of the same two SRH centres. We can apply the correlation between density and surface area to both types. Figure 10 shows lifetime per precipitate surface area versus excess minority carrier density with different majority carrier concentrations in (a) n-type silicon and (b) p-type silicon. For these calculations, we have taken $\eta_1\alpha_{p1} \approx 8 \times 10^3\,cm\,s^{-1}$ and $\eta_2\alpha_{p2} \approx 8 \times 10^6\,cm\,s^{-1}$ (as found from the Process A data based upon spherical precipitates) and we have applied these parameters to p-type silicon using the established values of $Q_1 = 157$ and $1/Q_2 = 1200$.[22]

At high excess minority carrier densities, the same "ambipolar" lifetime is reached in both the n-type and p-type cases for all majority carrier concentrations levels, as expected from SRH theory.[45,46] The ambipolar value is $\sim68\,\mu s\,cm^{-2}$. At lower excess minority carrier concentrations, the lifetime is dependent upon doping type and majority carrier concentration, as shown for some cases in Figures 10(a) and 10(b). The trend with majority carrier concentration is governed by Equation (5) for the n-type case and by an analogous expression for the p-type case. Figure 10(c) shows the ratio of the lifetime in n-type silicon to that in p-type silicon. For the ranges of conditions considered, the lifetime per unit surface area of the oxide precipitates is never lower in n-type silicon than in p-type silicon. At lower injections, we agree with Hwang and Schroder's conclusion that a given surface area of
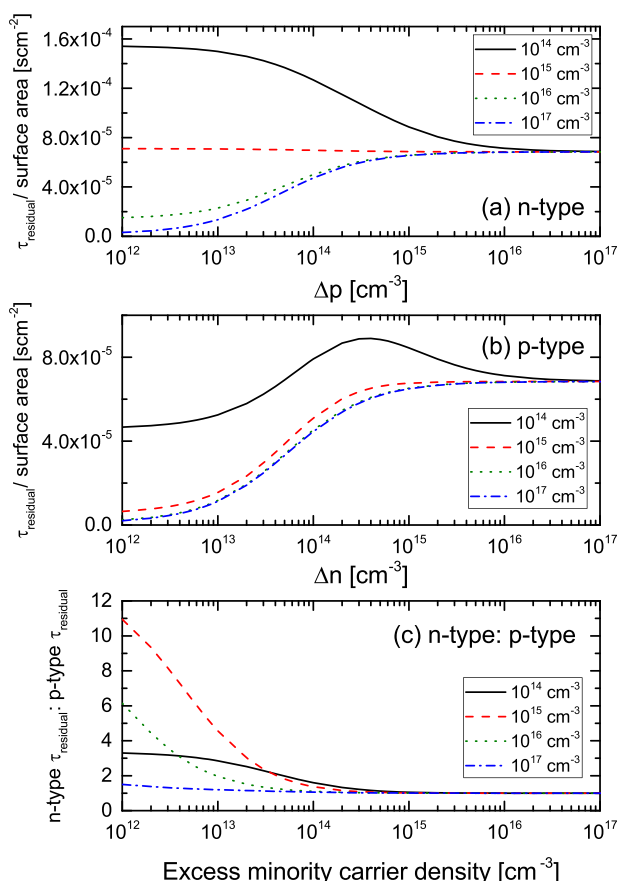
FIG. 10. Results of a simulation of minority carrier lifetime in *n*-type and *p*-type silicon with the four curves on each graph representing different values of majority carrier concentration. In (a) and (b) lifetime due to recombination at oxide precipitates per unit surface area of spherical oxide precipitates is plotted versus excess minority carrier density for *n*-type and *p*-type silicon, respectively. In (c) the ratio of the *n*-type lifetime to the *p*-type lifetime is plotted.

oxide precipitates is more detrimental to minority carrier lifetime in *p*-type silicon than in *n*-type silicon.[18] At higher injections, the lifetime in *n*-type and *p*-type silicon converge. Figure 10(c) indicates that the difference between *n*-type and *p*-type for practical photovoltaic operating conditions is close to negligible. For example for a doping level of 10^{16} cm^{-3} the lifetime variation between *n*-type and *p*-type is predicted to be <1% at an excess carrier density of 10^{15} cm^{-3} and ~10% at an excess carrier density of 10^{14} cm^{-3}.

V. CONCLUSIONS

The effect of oxide precipitates on minority carrier lifetime in *n*-type silicon has been studied. Two sets of samples were processed under substantially different conditions to create oxide precipitates with different characteristics for a given change in bulk oxygen concentration. The effect of surface recombination was considered and shown to be minimal, and external gettering was used to minimise the impurity concentration in the material.

Recombination at strained oxide precipitates in *n*-type silicon can be quantified in the same way we have previously demonstrated for *p*-type silicon. That is, the lifetime measured with silicon nitride surface passivation can be expressed

in terms of two independent SRH recombination centres, one with an energy level at $E_V + 0.22$ eV and a capture coefficient for electrons ~157 times greater than that for holes and the other with an energy level at $E_C - 0.08$ eV and a capture coefficient for holes ~1200 times greater than that for electrons. This parameterisation has been found to account for the lifetime in all samples considered, which have a range of doping levels and precipitate concentrations.

Injection-dependent minority carrier lifetime data have been correlated with bulk interstitial oxygen loss data from infrared absorption measurements and etching measurements which give strained oxide precipitate densities. The recombination parameters have been correlated with both precipitate density measurements and interface area estimates. While in one sample set the density of both states correlates with density and interface area, this is shown to be co-incidental. The use of a different sample set, in which a simple correlation between bulk interstitial oxygen loss and strained precipitate density does not occur, shows correlation with interface area and not density. We therefore conclude that the density of recombination centres associated with oxide precipitates is more likely to depend on their interface area. Based on this, we estimate the relative impact of oxide precipitates on minority carrier lifetime in *n*-type and *p*-type silicon. For a given interface area, the lifetime is never lower in *n*-type silicon than in *p*-type silicon, with the oxide precipitates being substantially more detrimental in the *p*-type case at lower injection levels.

[1]R. J. Falster and W. Bergholz, "The gettering of transition metals by oxygen-related defects in silicon," J. Electrochem. Soc. **137**, 1548 (1990).
[2]D. Gilles, E. R. Weber, and S. Hahn, "Mechanism of internal gettering of interstitial impurities in Czochralski-grown silicon," Phys. Rev. Lett. **64**, 196 (1990).
[3]W. Bergholz, M. J. Binns, G. R. Booker, J. C. Hutchison, S. H. Kinder, S. Messoloras, R. C. Newman, R. J. Stewart, and J. G. Wilkes, "A study of oxygen precipitation in silicon using high-resolution transmission electron microscopy, small-angle neutron scattering and infrared absorption," Philos. Mag. B **59**, 499 (1989).
[4]R. Falster, V. V. Voronkov, V. Y. Resnik, and M. G. Milvidskii, "Thresholds for effective internal gettering in silicon wafers," in *Proceedings of the Electrochemical Society, High Purity Silicon VIII* (2004), Vol. 200405, p. 188.
[5]V. V. Voronkov and R. Falster, "Grown-in microdefects, residual vacancies and oxygen precipitation bands in Czochralski silicon," J. Cryst. Growth **204**, 462 (1999).
[6]J. Haunschild, I. E. Reis, J. Geilker, and S. Rein, "Detecting efficiency-limiting defects in Czochralski-grown silicon wafers in solar cell production using photoluminescence imaging," Phys. Status Solidi RRL **5**, 199 (2011).
[7]K. Youssef, M. Shi, C. Radue, E. Good, and G. Rozgonyi, "Effect of oxygen and associated residual stresses on the mechanical properties of high growth rate Czochralski silicon," J. Appl. Phys. **113**, 133502 (2013).

[8]I. Kolevatov, V. Osinniy, M. Herms, A. Loshachenko, I. Shlyakhov, V. Kveder, and O. Vyvenko, "Oxygen-related defects: minority carrier lifetime killers in n-type Czochralski silicon wafers for solar cell application," Phys. Status Solidi C **12**, 1108 (2015).

[9]L. Chen, X. Yu, P. Chen, P. Wang, X. Gu, J. Lu, and D. Yang, "Effect of oxygen precipitation on the performance of Czochralski silicon solar cells," Sol. Energy Mater. Sol. Cells **95**, 3148 (2011).

[10]D. Song, J. Xiong, Z. Hu, G. Li, H. Wang, H. An, B. Yu, B. Grenko, K. Borden, K. Sauer, T. Roessler, J. Cui, H. Wang, J. Bultman, A. H. G. Vlooswijk, and P. R. Venema, paper presented at the 2012 38th IEEE Photovoltaic Specialists Conference (PVSC), Austin, TX (2012).

[11]F. Schindler, B. Michl, A. Kleiber, H. Steinkemper, J. Schön, W. Kwapil, P. Krenckel, S. Riepe, W. Warta, and M. C. Schubert, "Potential gain in multicrystalline silicon solar cell efficiency by n-type doping," IEEE J. Photovoltaics **5**, 499 (2015).

[12]D. Macdonald and L. J. Geerligs, "Recombination activity of interstitial iron and other transition metal point defects in p- and n-type crystalline silicon," Appl. Phys. Lett. **85**, 4061 (2004).

[13]F. E. Rougieux, B. Lim, J. Schmidt, M. Forster, D. Macdonald, and A. Cuevas, "Influence of net doping, excess carrier density and annealing on the boron oxygen related defect density in compensated n-type silicon," J. Appl. Phys. **110**, 063708 (2011).

[14]G. Coletti, P. Manshandena, S. Bernardini, P. C. P. Bronsveld, A. Gutjahra, Z. Hub, and G. Li, "Removing the effect of striations in n-type silicon solar cells," Sol. Energy Mater. Sol. Cells **130**, 647 (2014).

[15]K. H. Yang, H. F. Kappert, and G. H. Schwuttke, "Minority carrier lifetime in annealed silicon crystals containing oxygen," Phys. Status Solidi A **50**, 221 (1978).

[16]M. Miyagi, K. Wada, J. Osaka, and N. Inoue, "Effect of oxide precipitates on minority-carrier lifetime in Czochralski-grown silicon," Appl. Phys. Lett. **40**, 719 (1982).

[17]S. S. Chan, C. J. Varker, J. D. Whitfield, and R. W. Carpenter, "Deep levels associated with oxygen precipitation in Cz silicon and correlation with minority carrier lifetimes," Mater. Res. Soc. Symp. Proc. **46**, 281 (1985).

[18]J. M. Hwang and D. K. Schroder, "Recombination properties of oxygen-precipitated silicon," J. Appl. Phys. **59**, 2476 (1986).

[19]J. Vanhellemont, E. Simoen, A. Kaniava, M. Libezny, and C. Claeys, "Impact of oxygen related extended defects on silicon diode characteristics," J. Appl. Phys. **77**, 5669 (1995).

[20]F. G. Kirscht, Y. Furukawa, W. Seifert, K. Schmalz, A. Buczkowski, S. B. Kim, H. Abe, H. Koya, and J. Bailey, "Electrical characteristics of oxygen precipitation related defects in Czochralski silicon wafers," Mater. Sci. Eng. B **36**, 230 (1996).

[21]J. D. Murphy, K. Bothe, M. Olmo, V. V. Voronkov, and R. J. Falster, "The effect of oxide precipitates on minority carrier lifetime in p-type silicon," J. Appl. Phys. **110**, 053713 (2011).

[22]J. D. Murphy, K. Bothe, R. Krain, V. V. Voronkov, and R. J. Falster, "Parameterisation of injection-dependent lifetime measurements in semiconductors in terms of Shockley-Read-Hall statistics: an application to oxide precipitates in silicon," J. Appl. Phys. **111**, 113709 (2012).

[23]J. D. Murphy, K. Bothe, V. V. Voronkov, and R. J. Falster, "On the mechanism of recombination at oxide precipitates in silicon," Appl. Phys. Lett. **102**, 042105 (2013).

[24]J. D. Murphy, R. E. McGuire, K. Bothe, V. V. Voronkov, and R. J. Falster, "Minority carrier lifetime in silicon photovoltaics: The effect of oxygen precipitation," Sol. Energy Mater. Sol. Cells **120**, 402 (2014).

[25]M. Koizuka and H. Yamada-Kaneta, "Electron spin resonance centers associated with oxygen precipitates in Czochralski silicon crystals," J. Appl. Phys. **88**, 1784 (2000).

[26]V. Lang, J. D. Murphy, R. J. Falster, and J. J. L. Morton, "Spin-dependent recombination in Czochralski silicon containing oxide precipitates," J. Appl. Phys. **111**, 013710 (2012).

[27]W. Seifert, M. Kittler, M. Seibt, and A. Buczkowski, "Contrastive recombination behaviour of metal silicide and oxygen precipitates in n-type silicon: Attempt at an explanation," Solid State Phenom. **47–48**, 365 (1996).

[28]T. Mchedlidze and K. Matsumoto, "Electrically detected magnetic resonance signal from iron contaminated Czochralski silicon crystal," J. Appl. Phys. **83**, 4042 (1998).

[29]J. D. Murphy, R. E. McGuire, K. Bothe, V. V. Voronkov, and R. J. Falster, "Competitive gettering of iron in silicon photovoltaics: Oxide precipitates versus phosphorus diffusion," J. Appl. Phys. **116**, 053514 (2014).

[30]K. Bothe, R. J. Falster, and J. D. Murphy, "Room temperature sub-bandgap photoluminescence from silicon containing oxide precipitates," Appl. Phys. Lett. **101**, 032107 (2012).

[31]R. A. Sinton and A. Cuevas, "Contactless determination of current–voltage characteristics and minority-carrier lifetimes in semiconductors from quasi-steady-state photoconductance data," Appl. Phys. Lett. **69**, 2510 (1996).

[32]A. Richter, S. W. Glunz, F. Werner, J. Schmidt, and A. Cuevas, "Improved quantitative description of Auger recombination in crystalline silicon," Phys. Rev. B **86**, 165202 (2012).

[33]K. F. Kelton, R. Falster, D. Gambaro, M. Olmo, M. Cornara, and P. F. Wei, "Oxygen precipitation in silicon: Experimental studies and theoretical investigations within the classical theory of nucleation," J. Appl. Phys. **85**, 8097 (1999).

[34]F. S. Ham, "Theory of diffusion-limited precipitation," J. Phys. Chem. Solids **6**, 335 (1958).

[35]T. Y. Tan, L. L. Wu, and W. K. Tice, "Nucleation of stacking faults at oxide precipitate-dislocation complexes in silicon," Appl. Phys. Lett. **29**, 765 (1976).

[36]S. Senkader, J. Esfandyari, and G. Hobler, "A model for oxygen precipitation in silicon including bulk stacking fault growth," J. Appl. Phys. **78**, 6469 (1995).

[37]M. J. Kerr and A. Cuevas, "Recombination at the interface between silicon and stoichiometric plasma silicon nitride," Semicond. Sci. Technol. **17**, 166 (2002).

[38]D. R. Wight, I. D. Blenkinsop, W. Harding, and B. Hamilton, "Diffusion-limited lifetime in semiconductors," Phys. Rev. B **23**, 5495 (1981).

[39]A. Ourmazd and G. R. Booker, "The electrical recombination efficiency of individual edge dislocations and stacking fault defects in n-type silicon," Phys. Status Solidi A **55**, 771 (1979).

[40]K. Wada, N. Inoue, and K. Kohra, "Diffusion-limited growth of oxide precipitates in Czochralski silicon," J. Cryst. Growth **49**, 749 (1980).

[41]G. Hahn, M. Käs, and B. Herzog, "Hydrogenation in crystalline Silicon Materials for photovoltaic Application," Solid State Phenom. **156–158**, 343 (2009).

[42]E. Cartier, J. H. Stathis, and D. A. Buchanan, "Passivation and depassivation of silicon dangling bonds at the Si/SiO$_2$ interface by atomic hydrogen," Appl. Phys. Lett. **63**, 1510 (1993).

[43]R. C. Newman, M. J. Binns, W. P. Brown, F. M. Livingston, S. Messoloras, R. J. Stewart, and J. G. Wilkes, "Precipitation of oxygen in silicon: kinetics, solubility, diffusivity and particle size," Physica B **116**, 264 (1983).

[44]H. C. Sio, S. P. Phang, T. Trupke, and D. Macdonald, "Impact of phosphorous gettering and hydrogenation on the surface recombination velocity of grain boundaries in p-type multicrystalline silicon," IEEE J. Photovoltaics **5**, 1357 (2015).

[45]W. Shockley and W. T. Read, "Statistics of the recombinations of holes and electrons," Phys. Rev. **87**, 835 (1952).

[46]R. N. Hall, "Electron-hole recombination in germanium," Phys. Rev. **87**, 387 (1952).